

# CLEAR: A Semantic–Geometric Terrain Abstraction for Large-Scale Unstructured Environments

Pranay Meshram<sup>1</sup>, Charuvahan Adhivarahan<sup>1</sup>, Ehsan Tarkesh Esfahani<sup>2</sup>, Souma Chowdhury<sup>2</sup>, Chen Wang<sup>1</sup>, and Karthik Dantu<sup>1</sup>

**Abstract**—Long-horizon navigation in unstructured environments demands terrain abstractions that scale to tens of  $\text{km}^2$  while preserving semantic and geometric structure—a combination existing methods fail to achieve. Grids scale poorly; quadtrees misalign with terrain boundaries; neither encodes landcover semantics essential for traversability-aware planning. This yields infeasible or unreliable paths for autonomous ground vehicles operating over 10+  $\text{km}^2$  under real-time constraints. CLEAR (Connected Landcover Elevation Abstract Representation) couples boundary-aware spatial decomposition with recursive plane fitting to produce convex, semantically aligned regions encoded as a terrain-aware graph. Evaluated on maps spanning 9–100  $\text{km}^2$  using a physics-based simulator, CLEAR achieves up to 10× faster planning than raw grids with only 6.7% cost overhead and delivers 6–9% shorter, more reliable paths than other abstraction baselines. These results highlight CLEAR’s scalability and utility for long-range navigation for applications such as disaster response, defense, and planetary exploration.

## I. INTRODUCTION

Autonomous navigation in unstructured environments requires processing large, high-resolution maps of landcover and elevation, which is computationally prohibitive at scale. Traditional abstractions such as grid, hex, or quadtree discretizations simplify maps but often ignore semantic terrain boundaries and geometric structure, leading to inefficient planning or infeasible paths.

Consider autonomous wildfire response over 50  $\text{km}^2$  of mixed terrain. Grids are intractable at this scale; quadtrees ignore landcover, yielding routes that violate slope or friction constraints. Recent efforts in wildfire robotics [1]–[4] highlight the need for scalable terrain abstractions, yet rely on discretizations that sacrifice semantic or geometric fidelity. We target ground vehicles, whose mobility is directly constrained by slope, friction, and landcover—factors irrelevant to aerial systems. Unlike indoor scene graphs [5]–[9] with room-level structure, outdoor terrains exhibit continuous variation; CLEAR aligns regions with natural semantic and geometric boundaries.

<sup>1</sup>Department of Computer Science and Engineering, University at Buffalo, NY 14260, USA. {pmeshram, charuvah, cwx, kdantu}@buffalo.edu

<sup>2</sup>Department of Mechanical and Aerospace Engineering, University at Buffalo, NY 14260, USA. {ehsanesf, soumacho}@buffalo.edu

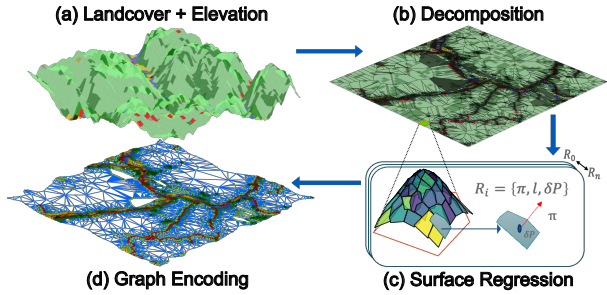


Fig. 1. The CLEAR framework takes in landcover and elevation data (a), applies boundary-seeded decomposition [Algorithm 1] (b), performs region-wise surface regression and abstraction [Algorithm 2] (c), and encodes connectivity through a graph representation over the resulting regions (d).

Connected Landcover Elevation Abstract Representation (CLEAR) decomposes terrain into convex, semantically coherent regions using boundary-seeded sampling and recursive plane fitting, then encodes them as a graph with terrain-aware costs. This enables efficient, reliable long-horizon planning.

CLEAR advances terrain abstraction through:

- 1) **Boundary-seeded decomposition:** Produces convex, semantically coherent regions via boundary-aware sampling and recursive plane fitting—the first method to jointly preserve landcover semantics and elevation geometry.
- 2) **Terrain-aware graph encoding:** Encodes slope and landcover for efficient cost-aware planning with standard graph search.
- 3) **Multi-scale validation:** Across 9–100  $\text{km}^2$  in physics-based simulation, CLEAR achieves 10× faster planning than raw grids with 6.7% cost overhead and 6–9% shorter paths than baselines.

## II. RELATED WORK

**Terrain Representation and Abstraction:** Classical abstractions such as grids [10], [11], hexagonal tilings [12], and quadtrees [10] simplify large maps but remain misaligned with semantic terrain boundaries. In contrast, indoor semantic scene graphs—e.g., 3D Scene Graph [5], [6], ConceptGraphs [7], and Hydra/Multi-Hydra [8], [9]—enable rich reasoning but operate at building scale with object- or room-level semantics.

CLEAR develops an analogous abstraction to outdoor terrains by coupling semantic landcover boundaries with elevation-derived geometry—a combination absent in prior work.

**Surface Simplification and Plane Fitting:** Surface-fitting models such as curved or planar patches [13], seed-curve fitting in agriculture [14], and adaptive quadtree surfaces [15] compactly approximate terrain geometry but ignore semantic consistency. CLEAR extends these ideas by applying recursive plane fitting within semantically coherent regions, preserving both geometric fidelity and semantic alignment.

**Path Planning on Abstract Maps:** Standard planners (A\* [10], RRT\* [16]) ignore terrain-specific costs like slope and friction. Geometry-aware abstractions such as HPPRM [17] and PUTN [18] improve terrain handling but lack semantic structure, while continuous surface maps [15] trade compactness for fidelity. Hierarchical methods like AMRA\* [19], [20] accelerate planning but remain grid-based and misaligned with outdoor terrain boundaries. CLEAR instead builds a region graph that is both terrain-aware and scalable to tens of  $\text{km}^2$ , enabling efficient and reliable long-horizon planning.

CLEAR unifies semantic and geometric terrain structure within a single abstraction, filling the gap between geometry-only surfaces and semantics-only maps.

### III. CONNECTED LANDCOVER ELEVATION ABSTRACT REPRESENTATION (CLEAR)

#### A. Problem Formulation

Let  $\Omega \subset \mathbb{R}^2$  denote the terrain. For each point  $p = (x, y) \in \Omega$ :

- $E(p) \in \mathbb{R}$  gives the elevation,
- $L(p) \in C$  gives the landcover class, where  $C = \{c_1, \dots, c_N\}$ .

CLEAR decomposes  $\Omega$  into a collection of convex, semantically coherent regions  $\{R_k\}_{k=1}^K$  produced by the Boundary-Seeded Decomposition (BSD) described in subsubsection III-B.1. Each region is then processed by recursive plane fitting, which may further subdivide  $R_k$  into planar subsets. Each resulting planar region is represented by:

$$R_k = (\pi_k, \mathcal{P}_k, c_k),$$

where  $\pi_k$  is the tangent plane fitted to the elevation values in that planar subset;  $\mathcal{P}_k$  is its polygonal boundary, coinciding with the original BSD polygon only when no subdivision is required; and  $c_k \in C$  is the dominant landcover label of the points belonging to that region. Each region satisfies:

- 1) *Geometric fidelity:* the RMSE between  $E$  and  $\pi_k$  over the region is below a tolerance  $\epsilon$ .
- 2) *Semantic uniformity:*  $c_k$  is the majority landcover label among the points in the region.

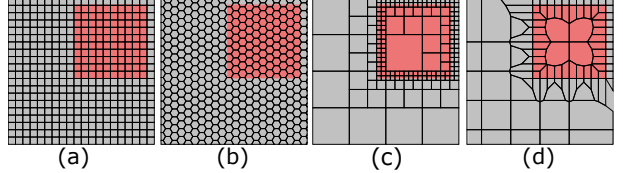


Fig. 2. Illustration of decomposition methods: (a) Grid — 400 cells, (b) Hexagonal — 448 cells, (c) Quadtree — 184 cells, (d) BSD — 105 cells.

3) *Structural convexity:* BSD ensures convex regions; recursive splitting produces convex subregions, each with boundary  $\mathcal{P}_k$ . Convexity enables discrete and continuous planning algorithms to be used on them for planning more seamlessly.

The final abstraction defines a region graph  $\mathcal{G} = (\mathcal{V}, \mathcal{E})$ , where vertices represent regions and edges encode traversable adjacency.

Attribute	Grid	Hex	Quadtree	BSD
[A1] Convex region support	✓	✓	✓	✓
[A2] Planner compatibility	✓	✓	✓	✓
[A3] Adaptive resolution	✗	✗	✓	✓
[A4] Compact representation	✗	✗	✓	✓
[A5] Semantic alignment	✗	✗	✗	✓
[A6] Geometry-aware fitting	✗	✗	✗	✓
[A7] Interpretability	✗	✗	✗	✓
[A8] Repeatability	✗	✗	✗	✓

TABLE I  
COMPARISON OF SPATIAL DECOMPOSITION STRATEGIES FOR TERRAIN ABSTRACTION. BOUNDARY SEEDED DECOMPOSITION (BSD) = BOUNDARY-SEED BASED DECOMPOSITION (PROPOSED).

✓ = SUPPORTED, ✗ = NOT SUPPORTED.

Table I compares decomposition strategies. BSD seeds regions at semantic boundaries and flat areas, then applies Voronoi tessellation.

#### B. CLEAR Design

CLEAR operates through: (1) *BSD*: region formation aligned with terrain boundaries, (2) *Plane Fitting*: geometric simplification within each region, and (3) *Graph Encoding*: building a region-level adjacency structure for planning tasks.

1) *Boundary-Seed Decomposition:* Boundary-Seed Decomposition (BSD) places seeds in flat regions and along high-entropy semantic boundaries, controlled by a priority factor  $\alpha_{\text{bdy}}$ . A Voronoi tessellation over these seeds produces convex regions aligned with natural land-cover and elevation boundaries. The complete procedure is given in Algorithm 1. **Intuition:** Place seeds preferentially in flat regions (low elevation variance) and along high-entropy landcover boundaries (controlled by  $\alpha_{\text{bdy}}$ ), then partition the region via Voronoi decomposition.

Fig. 2 shows BSD yields fewer, more coherent partitions than grid, hexagonal, or quadtree methods.

---

**Algorithm 1** Boundary-Seed Decomposition

---

**Require:**  $L \in \mathbb{Z}^{H \times W}$  (landcover map),  $E \in \mathbb{R}^{H \times W}$  (elevation map), target  $n$  (total seeds),  $\alpha_{\text{bdy}} \in [0, 1]$  (boundary priority),  $r_{\min}$  (minimum inter-seed distance),  $k$  (local entropy window size)

**Ensure:**  $\mathcal{S}$  with  $|\mathcal{S}| = n$

- 1:  $\sigma_E \leftarrow \text{LOCALSTD}_k(E)$ ;  $\tau_{\text{flat}} \leftarrow \text{quantile}_{0.25}(\sigma_E)$
- 2:  $B \leftarrow \text{BOUNDARYMASK}(L)$ ;  $H_k(p) \leftarrow \text{LOCALENTROPY}_k(L)$ ;  $R \leftarrow \text{argsort}_{p \in B}^{\downarrow} H_k(p)$
- 3:  $n_f \leftarrow n - (\alpha_{\text{bdy}} n)$ ;  $\mathcal{S} \leftarrow \emptyset$
- 4: **Uniform flat sampling:** visit pixels by ascending  $\sigma_E$ ; accept  $p$  if  $\min_{q \in \mathcal{S}} \|p - q\|_2 \geq r_{\min}$  until  $|\mathcal{S}| = n_f$
- 5: **Flat-region centroids:** for each label  $c$ , form connected components of  $\{\sigma_E \leq \tau_{\text{flat}}, L = c\}$ , add their centroids until  $|\mathcal{S}| \geq n_f$
- 6:  $m \leftarrow n - |\mathcal{S}|$ ; append the first  $m$  elements from  $R \setminus \mathcal{S}$  to  $\mathcal{S}$
- 7: **while**  $|\mathcal{S}| < n$  **do**
- 8:     append next elements from  $R \setminus \mathcal{S}$  to  $\mathcal{S}$
- 9: **end while**
- 10: **return** first  $n$  points of  $\mathcal{S}$

---

2) *Elevation Plane Fitting:* To capture terrain geometry, CLEAR approximates elevation within each BSD region using recursive planar fitting. A plane  $\pi_k$  is first fitted to the elevation values of the region; if the RMSE exceeds a tolerance  $\epsilon$ , the region is subdivided into four convex subregions and refitted. Each resulting planar patch inherits its dominant landcover label and is assigned a convex polygonal boundary obtained as the convex hull of its inlier points. This produces planar regions satisfying tolerance  $\epsilon$ . The full procedure is summarized in Algorithm 2.

**Complexity.** BSD runs in  $O(N \log N)$  for Voronoi construction. Recursive fitting terminates when RMSE  $\leq \epsilon$  or area  $< A_{\min} = 4$  pixels<sup>2</sup>, ensuring depth  $d \leq \lceil \log_4(A_0/A_{\min}) \rceil = O(\log N)$ , yielding  $O(N \log N)$  overall.

3) *Graph Encoding:* Planar regions form a graph  $G = (V, E)$ ; edges  $(v_i \rightarrow v_j)$  receive costs from Eq. (1), which incorporates slope, roughness, landcover, and heading alignment.

### C. Map Encoding for Terrain-Aware Path Planning

Each planar region is annotated with terrain attributes and a traversal cost to enable terrain-aware navigation.

#### 1) Encoded Attributes:

- *Percent Grade:* Magnitude of terrain slope; regions exceeding 35% grade are marked non-traversable.
- *Slope Direction (Aspect):* Orientation of steepest descent, used for slope-aligned and energy-efficient traversal.

---

**Algorithm 2** Recursive Planar Region Fitting with Landcover Labels

---

**Require:** 3D points  $\mathcal{X} = \{(x_i, y_i, z_i)\}_{i=1}^N$ , landcover labels  $\mathcal{L} = \{\ell_i\}_{i=1}^N$ , RMSE threshold  $\epsilon$

**Ensure:** Region set  $\mathcal{R} = \{(\pi_k, \mathcal{P}_k, c_k)\}$ , where  $\pi_k$  is a fitted plane,  $\mathcal{P}_k$  is a convex polygon (boundary of the planar patch), and  $c_k$  is the dominant landcover label

- 1: Initialize queue with  $(\mathcal{X}, \mathcal{L})$
- 2: **while** queue is not empty **do**
- 3:     Pop  $(\mathcal{X}_i, \mathcal{L}_i)$  from queue
- 4:     Fit plane  $\pi_i$  to points  $\mathcal{X}_i$  via least squares
- 5:     Compute RMSE:  $e_i = \text{RMSE}(Z, \pi_i)$
- 6:     **if**  $e_i \leq \epsilon$  or  $\mathcal{X}_i$  is spatially small **then**
- 7:          $\mathcal{P}_i \leftarrow \text{ConvexHull}(\mathcal{X}_i)$  // Clipped to parent
- 8:          $c_i \leftarrow \text{mode}(\mathcal{L}_i)$
- 9:         Append  $(\pi_i, \mathcal{P}_i, c_i)$  to  $\mathcal{R}$
- 10:     **else**
- 11:         Compute medians  $(x_m, y_m)$  of  $\mathcal{X}_i$
- 12:         Partition  $\mathcal{X}_i$  into quadrants  $\{\mathcal{X}_{i,k}\}_{k=1}^4$  using  $(x_m, y_m)$
- 13:         Push each  $(\mathcal{X}_{i,k}, \mathcal{L}_{i,k})$  to queue
- 14:     **end if**
- 15: **end while**
- 16: **return**  $\mathcal{R}$

---

- *Elevation Statistics:* Max/mean/min elevation values capturing local relief and terrain variability.
- *Landcover Type:* NALCMS class of the region, used to assign friction and roughness coefficients.

2) *Terrain-Aware Cost for Vehicle Path Planning:* We adapt [21]’s traversal model (distance, friction, slope, roughness). Unlike [21], we omit the steering-penalty term to avoid over-constraining long-range paths.

We introduce two extensions: (i) a **unified slope constraint**, marking regions with  $|s| > s_{\max}$  as non-traversable by setting  $\mathcal{C}_{\text{transfer}} = 10^{-6}$ ; and (ii) an **explicit slope-alignment penalty**,

$$\Delta\theta = \min(|\theta_{\text{head}} - \theta_{\text{slope}}|, 360 - |\theta_{\text{head}} - \theta_{\text{slope}}|), \quad (1)$$

This penalty favors perpendicular-to-slope traversal for stability and energy efficiency.

Edge cost follows [21]:  $C_{ij} = d_{ij}(1 + w_f \mu_{ij} + w_s |s_j| + w_r \sigma_j)$  with weights from [21], plus our heading penalty  $w_{\theta} \Delta\theta / 180^\circ$  with  $w_{\theta} = 0.1$ .

**Surface Coefficients.** Landcover classes are assigned friction/roughness coefficients per [21]–[23]; water and ice are marked non-traversable.

## IV. EVALUATION AND RESULTS

This section presents a comprehensive evaluation of the proposed CLEAR abstraction, thoroughly assess-

ing its structural, semantic, and functional performance through both quantitative metrics and qualitative analyses across diverse terrains.

We assess performance along three primary axes: (1) **Structural and semantic performance**, evaluating geometric fidelity, semantic consistency, and repeatability of the terrain abstraction; (2) **Path planning and executability**, benchmarking computational efficiency and path feasibility in simulation; and (3) **Ablation studies**, analyzing the sensitivity of decomposition parameters such as region count and boundary emphasis.

Unless otherwise specified, CLEAR is instantiated using Algorithm 1 for boundary-aware seeding (parameter  $\alpha_{\text{bdy}}$ ) and Algorithm 2 for recursive plane fitting (tolerance  $\varepsilon$ ). All experiments were conducted on a machine running Ubuntu 20.04 LTS with a 12th Gen Intel Core i9-12900K CPU and 32 GB RAM.

**Hyperparameters.** In Algorithm 1 (Boundary-Seeded Decomposition), two key parameters control the seed placement process. First, the *boundary emphasis* parameter  $\alpha_{\text{bdy}}$  balances between flatness-driven and boundary-driven seeding. It influences the distribution of regions but does not directly affect the planner. Empirically, increasing  $\alpha_{\text{bdy}}$  enhances boundary adherence and reconstruction fidelity, whereas lower values favor flatter interior regions and improved planning efficiency. To capture both aspects, we report decomposition-centric metrics using  $\alpha_{\text{bdy}} = 1$  and planning-centric results using  $\alpha_{\text{bdy}} = 0$ . These defaults balance reconstruction fidelity (high  $\alpha_{\text{bdy}}$ ) and planning efficiency (low  $\alpha_{\text{bdy}}$ ); ablations in Sec. IV-C explore this trade-off.

Second, the *flatness threshold*  $\tau_{\text{flat}}$  defines locally planar areas eligible for seed selection. We compute it as  $\tau_{\text{flat}} = P_{25}(\text{LOCALSTD}_{5 \times 5}(E))$ , corresponding to the flattest quartile (in meters). We set  $k = 3$  and  $r_{\min} = 2\text{--}4\text{ px}$  to minimize boundary mixing while maintaining uniform seed density.

$r_{\min}$  scales with pixel size, while  $k$  may be increased to 5 for stronger boundary discrimination.

In Algorithm 2 (Recursive Plane Fitting), the primary control parameter is the *planarity tolerance*  $\varepsilon$ , set to 10 m for 30 m DEMs. This threshold governs the termination of plane refinement and directly affects the trade-off between geometric accuracy and region compactness in the final abstraction.

Each of the following subsections details the corresponding evaluation setup, metrics, and results analysis.

### A. Structural and Semantic Performance

This subsection evaluates how effectively CLEAR preserves geometric structure and semantic composition across diverse terrains. Abstraction quality is assessed using three complementary metrics that capture structural fidelity and semantic consistency: the *Root*

*Mean Square Error (RMSE)* [24] for elevation reconstruction accuracy, the *mean Intersection-over-Union (mIoU)* [25]–[27] for semantic alignment, and the *repeatability ratio*, defined as the fraction of overlapping polygons with Intersection-over-Union (IoU)  $\geq 0.5$ , for spatial consistency.

**Dataset.** We construct a benchmark of 12 terrain tiles ( $100 \times 100$  pixels; each  $3\text{ km}^2$ ) sampled from Google Earth Engine. Each tile combines elevation data from the **NASADEM** dataset [28] and land-cover labels from the **North American Land Change Monitoring System (NALCMS)** [29], spanning homogeneous deserts to heterogeneous urban–vegetation regions. Terrain complexity is quantified by a combined score  $\Psi$ :

$$\Psi = \alpha \text{JSD}_{\text{norm}}(p) + (1 - \alpha)F, \quad (2)$$

where  $p$  is the empirical land-cover distribution,  $\text{JSD}_{\text{norm}}(p) = \sqrt{\text{JSD}(p\|u)}$  quantifies distributional diversity via Jensen-Shannon divergence from uniform  $u$ ,  $\alpha \in [0, 1]$  balances distributional and spatial components, and

$$F = \frac{1}{|\Omega|} \sum_{(i,j) \in \Omega} \frac{1}{k^2 - 1} \sum_{(u,v) \in \mathcal{N}_{ij}} \mathbb{1}[c_{i,j} \neq c_{u,v}]$$

measures local heterogeneity over neighborhood  $\mathcal{N}_{ij}$ . We set  $\alpha = 0.5$  and  $k = 5$  for balanced sensitivity to class diversity and spatial variation. Using this score, 12 tiles are selected to span the full range of terrain complexities—from homogeneous, low-entropy surfaces to highly heterogeneous urban–vegetation mixtures—ensuring unbiased evaluation across structural and semantic diversity.

**Geometric and Semantic Fidelity.** Elevation RMSE is computed between the original DEM and planar reconstructions from Algorithm 2, while mIoU measures agreement between reconstructed and ground-truth land-cover maps [30], [31]. Qualitative examples in Figure 4 and Figure 3 show that CLEAR produces contour-aligned, coherent regions that preserve both topographic structure and fine land-cover transitions, unlike Grid, Hexagonal, and Quadtree decompositions which exhibit blocky or misaligned artifacts. These observations highlight CLEAR’s strong **structural–semantic coupling**, yielding compact yet faithful abstractions.

Across varying terrain complexities, Figure 5 shows that CLEAR consistently maintains high semantic (mIoU) and geometric (low RMSE) fidelity, outperforming Grid, Hexagonal, and Quadtree decompositions. These results confirm that CLEAR generalizes effectively to heterogeneous and large-scale terrains, producing abstractions that are both semantically aligned and geometrically coherent.

**Repeatability.** We assess spatial consistency of the Boundary-Seeded Decomposition (BSD) against

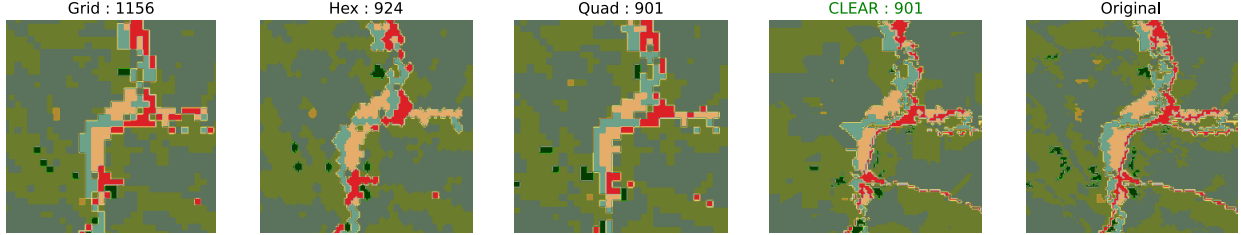


Fig. 3. Land-cover reconstruction on the Wharton (W) subregion. Grid, Hex, and Quadtree distort semantic boundaries, whereas CLEAR better preserves fine classes and irregular transitions.

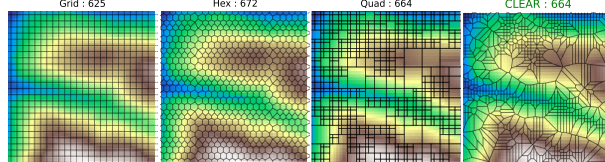


Fig. 4. Elevation reconstruction on the Wharton (W) subregion with  $\sim 650$  regions. CLEAR aligns with terrain contours and yields smooth planar regions, while Grid/Hex show stair-step artifacts and Quadtree exhibits block artifacts.

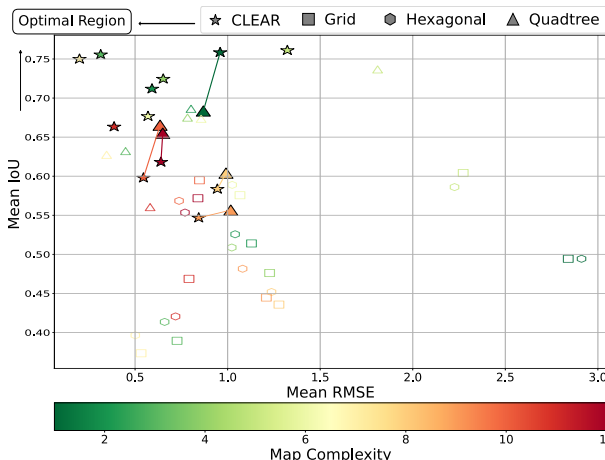


Fig. 5. Performance across 12 maps of varying complexity. Each point averages 5 decomposition resolutions. Axes report semantic fidelity (mIoU) and geometric fidelity (RMSE). CLEAR consistently outperforms Grid, Hexagonal, and Quadtree across all complexities.

Quadtree using ten 90%-overlapping patch pairs from Wharton (W). For each polygon in one patch, the best IoU-matched polygon in the adjacent patch is identified; polygons with  $\text{IoU} \geq 0.5$  are considered repeatable. Across 10 trials, BSD achieves  $0.97 \pm 0.005$  mean IoU and  $96.8 \pm 0.6\%$  repeatability, whereas Quadtree yields only  $0.39 \pm 0.01$  and  $4.5 \pm 3.8\%$ . This demonstrates that boundary-seeded regions remain stable under spatial shifts—essential for modular planning, map stitching, and multi-robot autonomy.

### B. Path Planning and Executability

This subsection evaluates how CLEAR’s abstraction improves path-planning efficiency and trajectory feasibility across diverse terrains. We first benchmark planning performance on abstracted versus raw maps, then validate executability through physics-based simulation. **Planning Efficiency.** Planning performance is evaluated

Map	Decomp.	Cost	Path Len (m)	P-Time(s)	A-Time(s)	Success(%)
W	A*	1.01	9114.9	0.46	—	—
	RRT*	394.88	9860.7	30.10	—	60.4
	Grid	1.13	9890.4	<b>0.16</b>	<b>31.52</b>	—
	Hex	<b>1.02</b>	8707.8	<u>0.22</u>	43.60	—
	Quadtree	1205.99	8494.2	<u>0.22</u>	44.93	—
	CLEAR	<u>1.05</u>	<b>9117.9</b>	0.23	<u>33.02</u>	—
H	A*	4.11	37502.7	8.06	—	—
	RRT*	7.67	38217.0	230.15	—	80.4
	Grid	4.78	42869.4	<u>0.91</u>	<b>305.15</b>	—
	Hex	<u>4.49</u>	38554.2	0.95	291.60	—
	Quadtree	129.23	37272.9	0.88	486.61	—
	CLEAR	<b>4.41</b>	<b>37735.8</b>	<b>0.87</b>	<b>284.27</b>	—
R	A*	7.21	64940.1	24.44	—	—
	RRT*	2606.82	57868.8	550.56	—	76.2
	Grid	9.08	80178.0	<u>1.46</u>	<b>631.44</b>	—
	Hex	<u>8.15</u>	68724.9	1.56	615.20	—
	Quadtree	532.46	64495.5	1.24	834.59	—
	CLEAR	<u>7.85</u>	<b>65708.3</b>	<u>1.25</u>	652.26	—

TABLE II

PLANNING PERFORMANCE ON W (WHARTON), H (HUMPHREYS), AND R (RAINIER). REPORTED: COST ( $\times 10^4$ ), PATH LENGTH (M), PLANNING TIME (P-TIME), ABSTRACTION TIME (A-TIME), AND RRT\* SUCCESS RATE. A\* AND RRT\* (SHADED) ARE NON-ABSTRACTION BASELINES. AMONG ABSTRACTION-BASED METHODS, CLEAR CONSISTENTLY ACHIEVES THE LOWEST COST AND COMPETITIVE PATH LENGTHS, WITH FASTER PLANNING AND LOWER ABSTRACTION TIMES THAN QUADTREE. REGION COUNTS: W=31,440, H=156,004, R=218,074.

using two metrics: (i) *planning time* for computational efficiency and (ii) *path cost* for feasibility and optimality. Experiments are conducted on three digital-twin terrains—**Wharton (W, 9 km<sup>2</sup>)**, **Humphreys (H, 50 km<sup>2</sup>)**, and **Mount Rainier (R, 100 km<sup>2</sup>)**—spanning different spatial scales and structural complexities. These terrain maps are extracted from Google Earth Engine using the same data pipeline described in subsection IV-A, ensuring consistent elevation (NASADEM) and land-cover (NALCMS) layers across scales. For each map, 10 diverse start-goal pairs are evaluated using the cost function defined in subsubsection III-C.2.

Table II shows, CLEAR yields the lowest planning cost among abstraction-based methods while maintaining path lengths comparable to A\*. On W, it nearly matches A\* (1.05 vs. 1.01), while Quadtree and RRT\* incur higher costs. Across H and R, CLEAR maintains this lead, achieving the lowest costs (4.41 and 7.85) with path lengths of 37.7 km and 65.7 km, respectively.



Fig. 6. (a) Multi-scale path-planning results on **W** ( $9\text{km}^2$ ), **H** ( $50\text{km}^2$ ), and **R** ( $100\text{km}^2$ ), showing vehicle paths from **CLEAR**, **Quadtree**, and **A\*** (optimal). (b) BeamNG simulation setup on **W** terrain map, with elevation and landcover rendered in-simulator to validate path executability and terrain consistency.

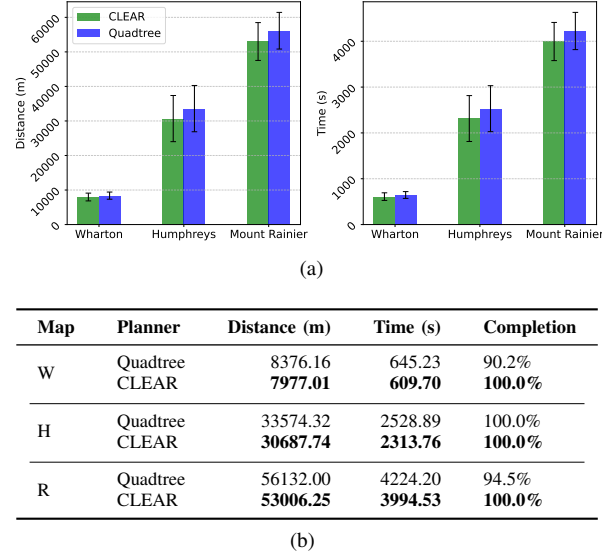


Fig. 7. Simulation-based executability on **W**, **H**, and **R** in BeamNG. (a) Mean path distance and execution time with error bars for pairs where both planners succeed. (b) Summary over all 10 pairs per map, reporting distance, execution time, and completion. CLEAR yields shorter, faster, and more reliable runs, with the largest gains on **R** where Quadtree fails grade constraints.

On **R**, it reduces cost by over 500 units relative to Quadtree, which frequently violates slope constraints. Although abstraction time increases with map size, CLEAR remains more efficient (284 s vs. 487 s on **H**; 652 s vs. 835 s on **R**), offering 2×–19× faster planning than **A\***, underscoring its scalability for long-horizon terrain-aware planning. The resulting vehicle trajectories across **W**, **H**, and **R** are shown in Figure 6(a), illustrating multi-scale path generation and the close agreement of CLEAR with the optimal **A\*** solutions.

**Executability in Simulation.** To validate physical feasibility, planned trajectories are executed in *BeamNG.tech* [32], a high-fidelity vehicle simulator with soft-body dynamics and heightfield terrains (Figure 6(b)). Each dataset map (W/H/R) is reconstructed from NASADEM elevation and rasterized landcover, preserving terrain friction and slope properties. Paths from Quadtree and CLEAR (30K regions) are executed using a PID speed–heading controller; runs are deemed successful if the vehicle reaches the goal within 2 m and 15°. For each map, the same 10 start–goal pairs are

simulated to ensure consistency between planning and execution trials.

Across all terrains, CLEAR shortens path length by an average of **6.3%** (max **8.6%** on **H**) and reduces execution time by **6.5%** (max **8.5%** on **H**) compared to Quadtree. On **R**, Quadtree frequently fails due to exceeding the **35%** grade constraint, while CLEAR completes all runs successfully. Even when restricted to cases where both planners succeed (7a, 7b), CLEAR consistently produces shorter, faster, and smoother trajectories.

Overall, these results confirm that CLEAR’s structure-aware abstraction accelerates planning while maintaining dynamic feasibility, enabling scalable, executable navigation across complex terrains.

### C. Ablation Studies

This subsection analyzes how key parameters influence CLEAR’s decomposition and planning performance. We ablate two main factors: (i) the *region budget*, which controls abstraction granularity for fair cross-method comparison, and (ii) the *boundary emphasis* parameter  $\alpha_{bdy}$ , which governs seed placement in Algorithm 1. All experiments are conducted on **W**.

**Region Budget – Decomposition.** Figure 8(a-c) analyzes how varying the region count influences reconstruction quality across Grid, Hexagonal, Quadtree, and CLEAR. Region counts are standardized using Quadtree’s minimum-area thresholds {16, 8, 4, 2, 1} and matched across all methods for fairness. In elevation RMSE (Figure 8 a), CLEAR achieves the lowest error with significantly fewer regions, demonstrating high geometric fidelity. For landcover mIoU (Figure 8 b), it consistently outperforms Grid and Hexagonal and matches or surpasses Quadtree, maintaining strong semantic alignment. Global information retention, measured via JSD (Figure 8 c), further confirms that CLEAR produces compact, information-preserving representations with minimal loss. Together, these results show that CLEAR sustains both geometric and semantic integrity under coarse abstractions, achieving higher efficiency per region and better scalability than existing methods.

**Region Budget – Planning.** The rightmost plot in

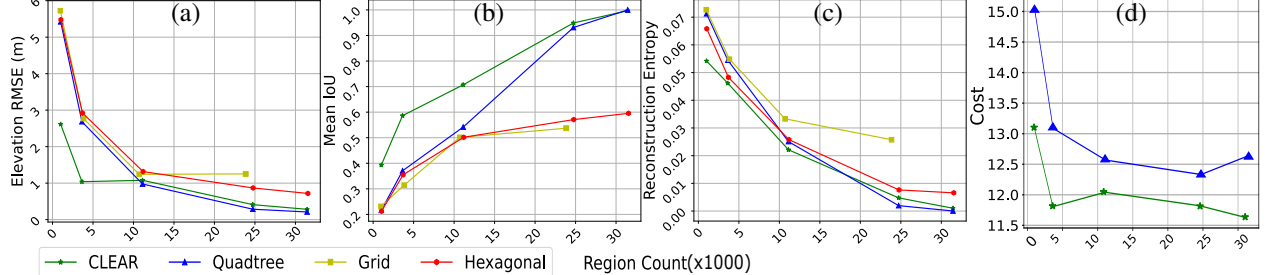


Fig. 8. Reconstruction and planning evaluation on W. (a–c) Decomposition metrics: RMSE, mIoU, and JSD vs. region count. (d) Planning cost vs. region count. CLEAR achieves the best fidelity–compactness balance and consistently yields lower-cost paths at coarse scales.

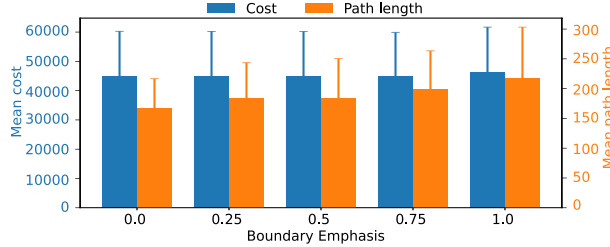


Fig. 9. Ablation of the *Boundary Emphasis*  $\alpha_{\text{bdy}} \in [0, 1]$  in the decomposition stage. Left axis: mean planning cost; right axis: mean path length.  $\alpha_{\text{bdy}}=0$  is flatness-only seeding,  $\alpha_{\text{bdy}}=1$  is boundary-only seeding. Error bars denote standard deviation across 10 goal-start pair.

Figure 8(d) shows path cost versus region count on W using Dijkstra’s algorithm. CLEAR consistently yields lower-cost paths, particularly at low resolutions where Quadtree’s irregular boundaries reduce connectivity. While all methods improve with increasing regions, CLEAR maintains a clear advantage, indicating that its structure-preserving abstraction delivers superior planning fidelity even under tight region budgets.

**Boundary Emphasis**  $\alpha_{\text{bdy}}$ . On the medium-scale terrain (H), we ablate the boundary weighting parameter  $\alpha_{\text{bdy}} \in [0, 1]$ , which balances boundary adherence and interior flatness in Algorithm 1. Path-planning performance is evaluated over 10 start–goal pairs for abstractions generated at each setting. Higher  $\alpha_{\text{bdy}}$  improves boundary alignment and reconstruction fidelity but slightly increases path cost, while smaller values favor flatter regions and shorter paths with minor semantic loss. For the main results, we use  $\alpha_{\text{bdy}} = 0$  for planning-focused experiments and  $\alpha_{\text{bdy}} = 1$  to demonstrate maximal reconstruction fidelity.

## V. DISCUSSION

**Limitations and Failure Modes.** CLEAR assumes obstacle-free terrain; rigid clutter (boulders, logs) is masked as non-traversable rather than modeled explicitly. This is overly conservative for human navigation where small obstacles are traversible. Regions smaller than  $r_{\min}$  fail to form coherent boundaries, degrading performance in extremely fragmented terrain (e.g., dense urban or rocky outcrops). Computational cost scales with point density; downsampling reduces fidelity but enables real-time processing on embedded systems.

**Convexity and Optimality.** BSD guarantees convex regions via Voronoi tessellation, and recursive splitting preserves convexity through axis-aligned partitioning. Each region is GCS-compatible, enabling continuous trajectory optimization [33]. However, CLEAR does not guarantee global optimality: discretization error ( $\varepsilon$ ) trades path quality for compactness. Our results show this overhead is  $< 7\%$ , which is acceptable for real-time, long-range planning where a  $10\times$  speedup is critical.

**Future Directions.** Incremental updates could exploit BSD’s repeatability (96.8% IoU) for distributed multi-robot mapping. Obstacle-aware masking could incorporate agent-specific clearance models for heterogeneous teams. Each region’s convexity enables GCS-based trajectory optimization for globally optimal continuous paths. Potential applications include wildfire response (our motivating example), search-and-rescue over  $50+\text{ km}^2$ , and planetary exploration where bandwidth limits preclude raw map transmission.

## VI. CONCLUSION

We introduced CLEAR, a boundary-aware terrain abstraction that couples semantic boundaries with recursive plane fitting to produce compact, faithful region graphs for large-scale planning. Across tiles spanning diverse semantic compositions and structural complexities, CLEAR achieves high semantic fidelity (mIoU) and low geometric error (RMSE), outperforming grid, hexagonal, and quadtree abstractions. In planning and execution, CLEAR yields up to 8.6% shorter paths and nearly 10% higher task success in closed-loop physics-based simulation. Compared to a non-abstraction baseline (A\*), CLEAR plans roughly  $10\times$  faster with only about 7% cost overhead, while maintaining path lengths within 1.3% of A\* across maps.

These results demonstrate that CLEAR enables efficient, reliable long-horizon navigation for disaster response, planetary exploration, and defense applications requiring real-time planning over  $10+\text{ km}^2$ .

## REFERENCES

- [1] E. Seraj, A. Silva, and M. Gombolay, “Multi-uav planning for cooperative wildfire coverage and tracking with quality-of-service guarantees,” *Autonomous Agents and Multi-Agent Systems*, vol. 36, no. 2, p. 39, 2022.

[2] M. Al-Husseini, K. H. Wray, and M. J. Kochenderfer, "Hierarchical framework for optimizing wildfire surveillance and suppression using human-autonomous teaming," *Journal of Aerospace Information Systems*, vol. 21, no. 10, pp. 790–811, 2024.

[3] S. Martínez-Rozas, R. Rey, D. Alejo, D. Acedo, J. A. Cobano, A. Rodríguez-Ramos, P. Campoy, L. Merino, and F. Caballero, "An aerial/ground robot team for autonomous firefighting in urban gnss-denied scenarios," *Field Robotics*, vol. 2, pp. 241–273, 2022.

[4] K. Jindal, A. Wang, D. Thakur, A. Zhou, V. Spurny, V. Walter, G. Broughton, T. Krajnik, M. Saska, and G. Loianno, "Design and deployment of an autonomous unmanned ground vehicle for urban firefighting scenarios," *Field Robotics*, vol. 1, pp. 1–17, 2021.

[5] I. Armeni, Z.-Y. He, J. Gwak, A. R. Zamir, M. Fischer, J. Malik, and S. Savarese, "3d scene graph: A structure for unified semantics, 3d space, and camera," in *Proceedings of the IEEE/CVF International Conference on Computer Vision (ICCV)*, October 2019.

[6] J. Strader, N. Hughes, W. Chen, A. Speranzon, and L. Carlone, "Indoor and outdoor 3d scene graph generation via language-enabled spatial ontologies," *IEEE Robotics and Automation Letters*, vol. 9, no. 6, pp. 4886–4893, 2024.

[7] Q. Gu, A. Kuwajerwala, S. Morin, K. M. Jatavallabhula, B. Sen, A. Agarwal, C. Rivera, W. Paul, K. Ellis, R. Chellappa, C. Gan, C. M. de Melo, J. B. Tenenbaum, A. Torralba, F. Shkurti, and L. Paull, "Conceptgraphs: Open-vocabulary 3d scene graphs for perception and planning," in *2024 IEEE International Conference on Robotics and Automation (ICRA)*, 2024, pp. 5021–5028.

[8] N. Hughes, Y. Chang, and L. Carlone, "Hydra: A real-time spatial perception system for 3d scene graph construction and optimization," *arXiv preprint arXiv:2201.13360*, 2022.

[9] Y. Chang, N. Hughes, A. Ray, and L. Carlone, "Hydra-multi: Collaborative online construction of 3d scene graphs with multi-robot teams," in *2023 IEEE/RSJ International Conference on Intelligent Robots and Systems (IROS)*. IEEE, 2023, pp. 10995–11002.

[10] P. E. Hart, N. J. Nilsson, and B. Raphael, "A formal basis for the heuristic determination of minimum cost paths," in *IEEE Transactions on Systems Science and Cybernetics*, vol. SSC-4, no. 2, 1968, pp. 100–107.

[11] D. Ball *et al.*, "Vision-based obstacle detection and navigation for an agricultural robot," *Journal of Field Robotics*, vol. 33, no. 8, pp. 1107–1130, 2016.

[12] P. Duszak, B. Siemiatkowska, and R. Wieckowski, "Hexagonal grid-based framework for mobile robot navigation," *Remote Sensing*, vol. 13, no. 21, p. 4216, 2021.

[13] D. Kanoulas, N. G. Tsagarakis, and M. Vona, "Curved patch mapping and tracking for irregular terrain modeling," *Robotics and Autonomous Systems*, vol. 119, pp. 13–30, 2019.

[14] J. Jin and L. Tang, "Coverage path planning on three-dimensional terrain for arable farming," *Journal of Field Robotics*, vol. 28, no. 3, pp. 424–440, 2011.

[15] Y. Zhang and S. Wang, "An optimization-based robot navigation system in complex terrain on a hybrid map," *IEEE Transactions on Vehicular Technology*, 2025.

[16] S. Karaman and E. Frazzoli, "Sampling-based algorithms for optimal motion planning," *The International Journal of Robotics Research*, vol. 30, no. 7, pp. 846–894, 2011.

[17] A. Ravankar, A. Ravankar, T. Emara, and Y. Kobayashi, "Hpprm: Hybrid potential based probabilistic roadmap algorithm for improved dynamic path planning of mobile robots," *IEEE Access*, vol. 8, pp. 221743–221766, 2020.

[18] Z. Jian *et al.*, "Putn: A plane-fitting based uneven terrain navigation framework," *IEEE/RSJ International Conference on Intelligent Robots and Systems (IROS)*, pp. 7160–7166, 2022.

[19] M. Likhachev, G. J. Gordon, and S. Thrun, "Ara\*: Anytime a\* with provable bounds on sub-optimality," *Advances in neural information processing systems*, vol. 16, 2003.

[20] D. M. Saxena, T. Kusnur, and M. Likhachev, "Amra\*: Anytime multi-resolution multi-heuristic a\*," in *2022 International Conference on Robotics and Automation (ICRA)*, 2022, pp. 3371–3377.

[21] T. Fu, Z. Zhan, Z. Zhao, S. Su, X. Lin, E. T. Esfahani, K. Dantu, S. Chowdhury, and C. Wang, "Anynav: Visual neuro-symbolic friction learning for off-road navigation," *arXiv preprint arXiv:2501.12654*, 2025.

[22] K. B. Pandolf, B. Givoni, and R. F. Goldman, "Predicting energy expenditure with loads while standing or walking very slowly," *Journal of Applied Physiology*, vol. 43, no. 4, pp. 577–581, 1977.

[23] P. Papadakis, "Terrain traversability analysis methods for unmanned ground vehicles: A survey," *Engineering Applications of Artificial Intelligence*, vol. 26, no. 4, pp. 1373–1385, 2013.

[24] V.-C. Miclea and S. Nedevschi, "Monocular Depth Estimation With Improved Long-Range Accuracy for UAV Environment Perception," *IEEE Transactions on Geoscience and Remote Sensing*, vol. 60, pp. 1–15, 2022. [Online]. Available: <https://ieeexplore.ieee.org/document/9372395>

[25] X. Lai, Z. Tian, L. Jiang, S. Liu, H. Zhao, L. Wang, and J. Jia, "Semi-supervised Semantic Segmentation with Directional Context-aware Consistency," in *2021 IEEE/CVF Conference on Computer Vision and Pattern Recognition (CVPR)*. Nashville, TN, USA: IEEE, Jun. 2021, pp. 1205–1214. [Online]. Available: <https://ieeexplore.ieee.org/document/9578346>

[26] A. Valada, R. Mohan, and W. Burgard, "Self-Supervised Model Adaptation for Multimodal Semantic Segmentation," *International Journal of Computer Vision*, vol. 128, no. 5, pp. 1239–1285, May 2020. [Online]. Available: <http://link.springer.com/10.1007/s11263-019-01188-y>

[27] C. Kamann and C. Rother, "Benchmarking the Robustness of Semantic Segmentation Models," in *2020 IEEE/CVF Conference on Computer Vision and Pattern Recognition (CVPR)*. Seattle, WA, USA: IEEE, Jun. 2020, pp. 8825–8835. [Online]. Available: <https://ieeexplore.ieee.org/document/9157010>

[28] N. J. P. Laboratory, "Nasadem: Nasa shuttle radar topography mission global 1 arc second v001," <https://doi.org/10.5067/MEaSUREs/NASADEM/NASADEM.HGT.001>, 2020, accessed via Google Earth Engine.

[29] C. for Environmental Cooperation (CEC), "North american land change monitoring system (nalcms) land cover 2015, 30m," <https://www.cec.org/nalcms/>, 2020, accessed via Google Earth Engine.

[30] M. Cordts, M. Omran, S. Ramos, T. Rehfeld, M. Enzweiler, R. Benenson, U. Franke, S. Roth, and B. Schiele, "The Cityscapes Dataset for Semantic Urban Scene Understanding," in *2016 IEEE Conference on Computer Vision and Pattern Recognition (CVPR)*. Las Vegas, NV, USA: IEEE, Jun. 2016, pp. 3213–3223. [Online]. Available: <http://ieeexplore.ieee.org/document/7780719/>

[31] M. Everingham, S. M. A. Eslami, L. Van Gool, C. K. I. Williams, J. Winn, and A. Zisserman, "The Pascal Visual Object Classes Challenge: A Retrospective," *International Journal of Computer Vision*, vol. 111, no. 1, pp. 98–136, Jan. 2015. [Online]. Available: <http://link.springer.com/10.1007/s11263-014-0733-5>

[32] BeamNG GmbH, "BeamNG.tech." [Online]. Available: <https://www.beamng.tech/>

[33] T. Marcucci, J. Umenberger, P. Parrilo, and R. Tedrake, "Shortest paths in graphs of convex sets," *SIAM Journal on Optimization*, vol. 34, no. 1, pp. 507–532, 2024.